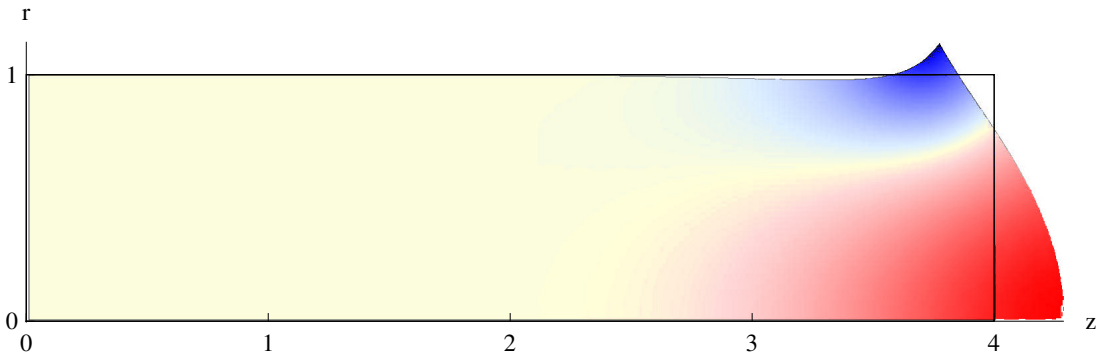

Figure 9.1 page 142. Demonstration of Saint-Venant's principle. A circular cylinder with radius $a = 1$ and length $L = 4$ is placed with its z-axis as shown. You should rotate the figure around the z-axis to see the three-dimensional image. The originally relaxed cylinder is loaded at the right end with a radially varying pressure distribution $p_z = -\sigma_{zz} = 2r^2 - 1$, for which both the total force and total moment of force on the cylinder vanish. Young's modulus is taken to be 1000, and Poisson's ratio 1/3. The colors indicate the pressure p_z along z in the cylinder, with red being positive (compression) and blue negative (extension). The pressure distribution is seen to extend less than one diameter from the right end, in accordance with Saint-Venant's principle. The surface deformation is strongly exaggerated.

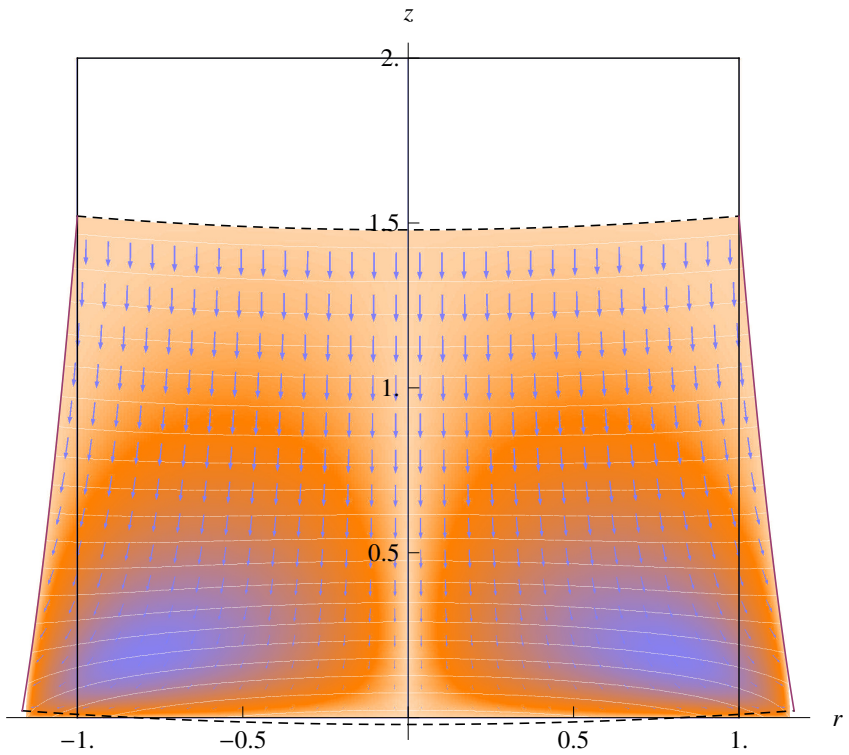

Figure 9.2 page 144. Numeric solution to the gravitational settling of a cylindrical block of fairly soft material ("jelly"). The square outline marks the undeformed shape with radius $a = 1$ and height $h = 2$, Poisson's ratio $\nu = 1/3$, and deformation scale $D = E/\rho_0 g_0 = 4$. The image is a cut through the rz-plane and should be rotated around the vertical z-axis. The arrows are proportional to the displacement field. The colored background indicates shear stress, $\sigma_{rz} = \sigma_{zr}$, with blue being high and orange low. The fully drawn and nearly horizontal lines are isobars for the vertical pressure, $p_z = -\sigma_{zz}$, showing that towards the bottom it is higher in the middle than at the edges. The dashed lines indicate the shape of the deformed block in the shear-free approximation, normalized to vanishing average vertical displacement at $z = 0$. The agreement between model and data is quite impressive.

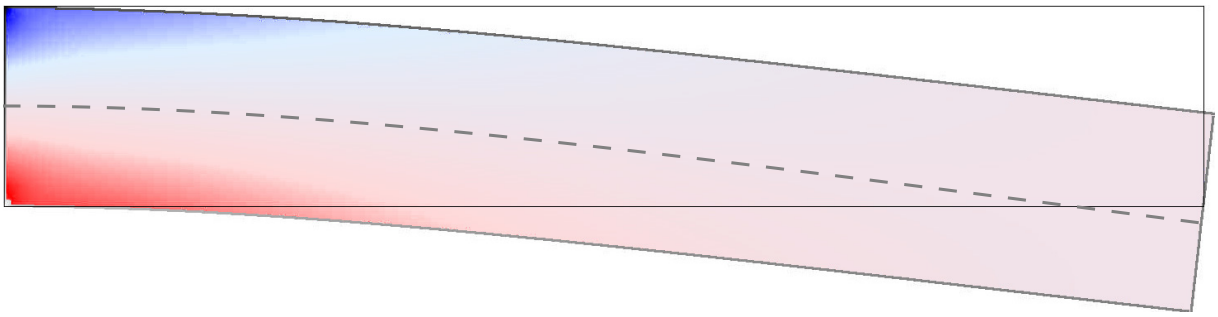

Figure 10.1 page 165. Simulation of cantilever bent by its own weight. The undeformed shape is outlined in dark. In arbitrary units (for example SI), the cantilever has length $L = 6$ and a quadratic cross-section with side lengths 1, yielding an area moment $I = 1/12$. Young's modulus is $E = 10^4$ and the weight per unit of length $K = 3$. The colors indicate the values of longitudinal pressure, $p_z = -\sigma_{zz}$, and clearly show that the rod's material is stretched on the upper side and compressed at the lower. The dashed line, which follows the central ray perfectly, is the slender rod prediction CM-(10.8).

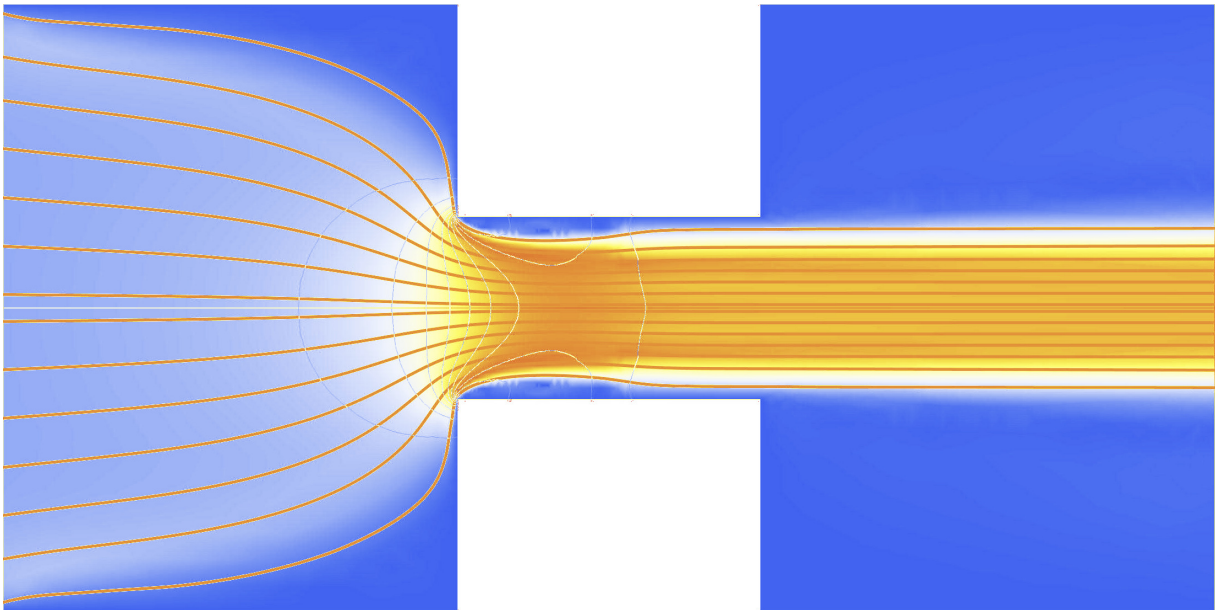

Figure 13.2 page 211. Two-dimensional simulation of nearly ideal steady flow through a channel (in the absence of gravity). The Reynolds number is about 500. The incompressible fluid enters at the left of the image under uniform pressure and exits at the right with a lower, also uniform, pressure. The gray-level represents the speed of the fluid, and the streamlines indicate the flow direction as well as the flow speed (by their density). Pressure contours are also shown and generally cross the streamlines. There are clearly visible boundary layers near the walls of the narrow channel, and the uniformly spaced streamlines indicate that there is nearly homogeneous flow in the central region of the channel and in the outlet jet. The boundary layers separate from the channel walls at the outlet and continue along the two edges of the jet, slowly causing it to widen. Near the walls of the exit region there is a weak secondary flow running against the main flow. For decreasing viscosity—or better, for increasing Reynolds number—this general picture will persist, although the boundary layers become progressively thinner until turbulence unavoidably sets in (see Chapter CM-28).

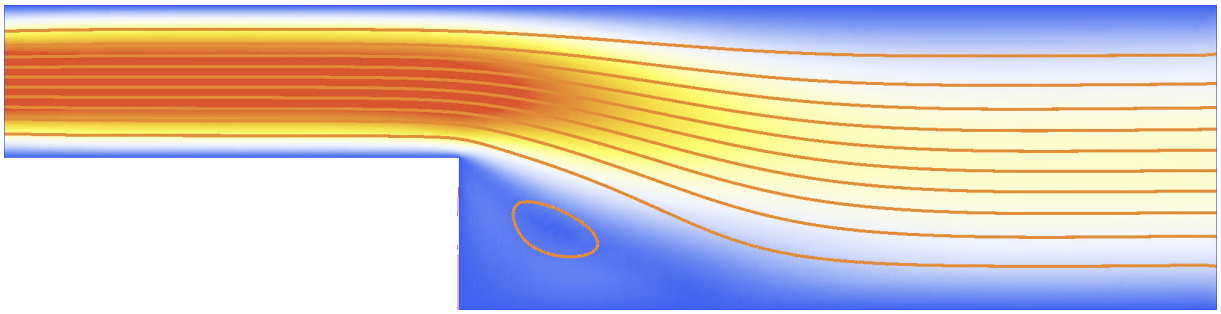

Figure 13.3 page 217. Two-dimensional flow over a backstep in a channel at Reynolds number 500. The streamlines coming in from the left do not cover the whole volume of fluid because a whirl has formed behind the step. The color indicates the magnitude of the velocity field. Some viscosity is necessary to make the simulation work, so this is not truly ideal but only nearly ideal flow well away from the solid boundaries.

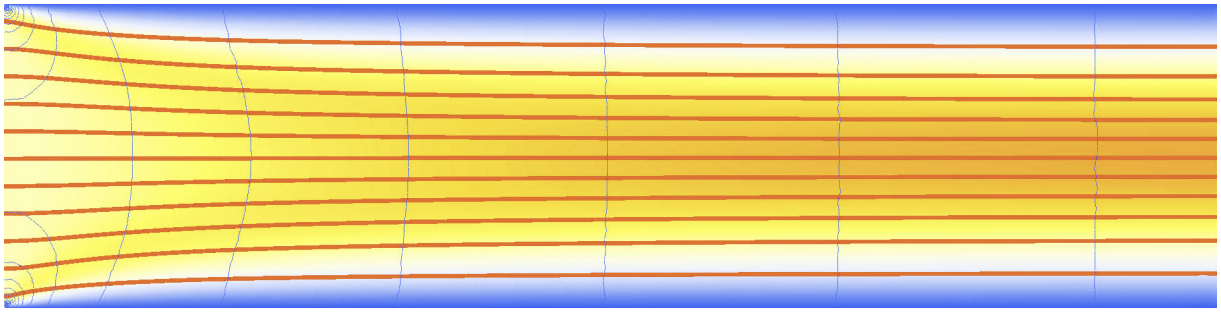

Figure Margin page 265. Simulation of channel entrance flow at $\mathsf{Re} = 100$. The flow enters from above with uniform velocity and settles into the parabolic solution CM-(16.5) downstream from the entry. The background color indicates the magnitude of the velocity $|\boldsymbol{v}|$, the longitudinal curves are the streamlines, and the crossing curves are pressure contours.

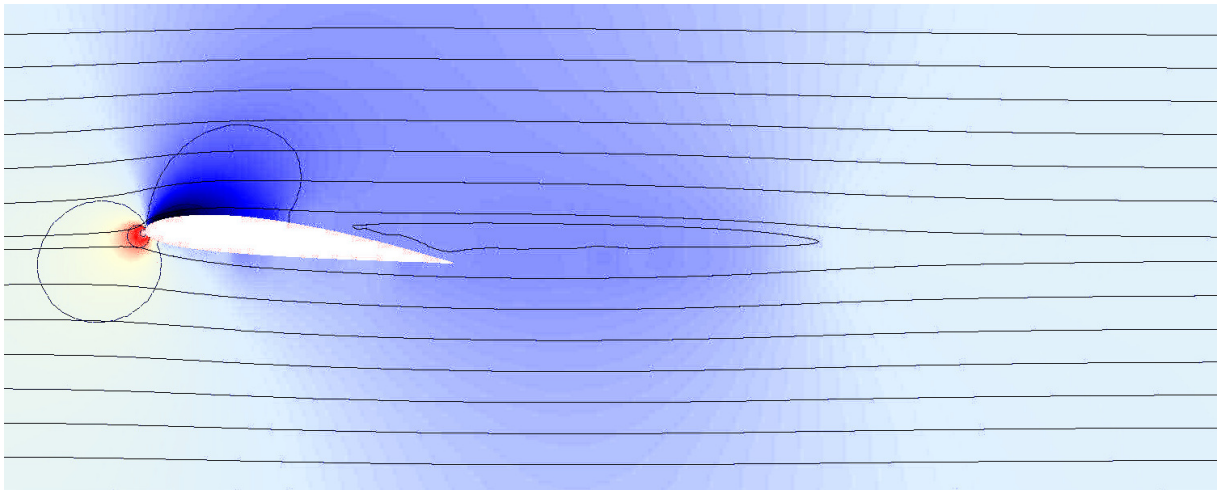

Figure 29.3 page 523. Pressure distribution around a NACA2412 airfoil at Reynolds number $\mathsf{Re}_c = 10,000$ and angle of attack $\alpha = 6°$. The stagnation pressure is high (red) at the leading edge and the lifting pressure low (blue) above the the wing. The lifting pressure typically acts on top of the wing about one quarter of the chord length downstream from the leading edge, as can be seen by the darker coloring in this region and the blue isobars. The rest of the airfoil is basically there to secure an orderly departure of the air from the wing. The streamlines show that the high angle of attack has caused boundary layer separation with reversed flow above the trailing edge, stretching quite far behind.

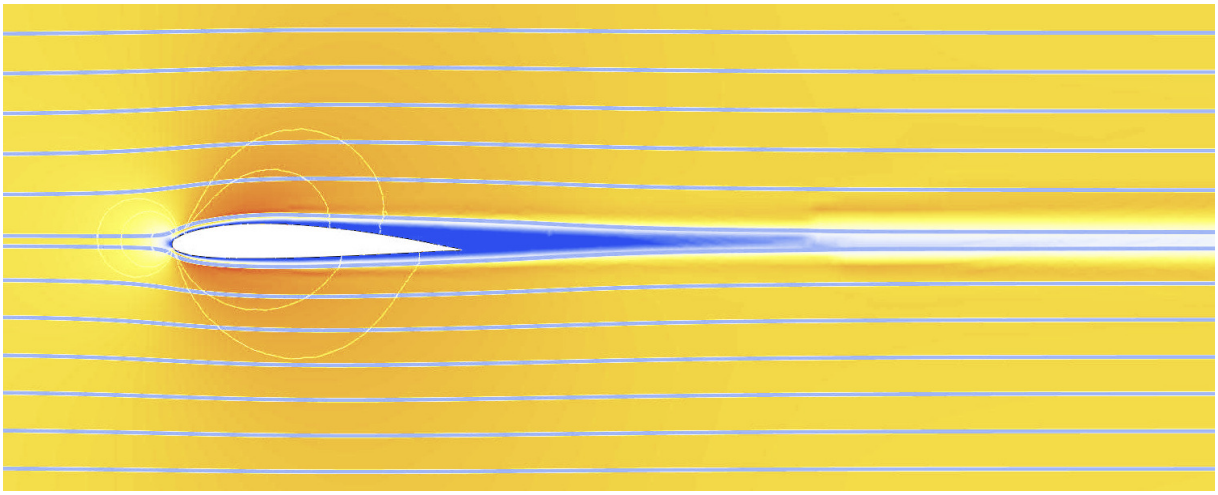

Figure 29.6 page 529. Velocity distribution ($|\boldsymbol{v}|$) around a NACA2412 airfoil at Reynolds number $\mathsf{Re}_c = 10{,}000$ and angle of attack $\alpha = 1°$. Note the stagnating flow at the leading edge (lighter), and the strong slowdown of the flow in the boundary layers and the trailing wake (blue). A few isobars are also shown (yellow). The boundary layers are thin and laminar and thicken toward the rear, especially on the upper surface where the initial acceleration of the air is followed by deceleration. There is essentially no turbulence in the boundary layers at a Reynolds number as low as this. At more realistic Reynolds numbers in the millions, the boundary layers are mostly turbulent and about an order of magnitude thinner than here. Well behind the airfoil the wake has a thickness comparable to the boundary layers. The slow viscous expansion of the laminar wake is not visible at the scale of this figure.